ACS Catalysis

Research Article

pubs.acs.org/acscatalysis

Mechanism and Activity of Water Oxidation on Selected Surfaces of Pure and Fe-Doped NiO_x

Ye-Fei Li* and Annabella Selloni*

Department of Chemistry, Princeton University, Princeton, New Jersey 08544, United States

Supporting Information

ABSTRACT: Mixed nickel–iron oxides have recently emerged as promising electrocatalysts for water oxidation because of their low cost and high activity, but the composition and structure of the catalyst's active phase under working conditions are not yet fully established. We present here density functional theory calculations with on-site Coulomb repulsion of the energetics of the oxygen evolution reaction (OER) on selected surfaces of pure and mixed Ni–Fe oxides that are possible candidates for the catalyst's active phase. The investigated surfaces are pure β-NiOOH(01$\bar{1}$5) and γ-NiOOH(101), Fe-doped β-NiOOH(01$\bar{1}$5) and γ-NiOOH(101), $NiFe_2O_4$(001), and Fe_3O_4(001). We find that Fe-doped β-NiOOH(01$\bar{1}$5) has by far the lowest overpotential (η = 0.26 V), followed by $NiFe_2O_4$(001) (η = 0.42 V). Our results indicate that Fe-doped β-NiOOH and, to a lesser extent, $NiFe_2O_4$ could be the phases responsible for the enhanced OER activity of NiO_x when it is doped with Fe.

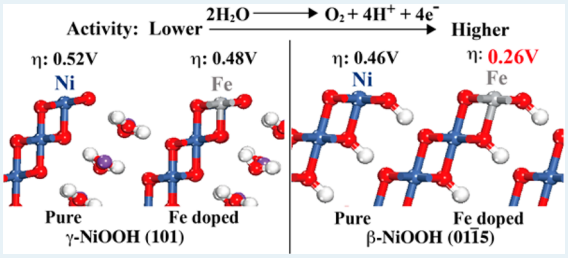

KEYWORDS: *water oxidation, electrocatalysis, DFT, mixed Ni–Fe oxides, active phases*

1. INTRODUCTION

As a prototype reaction for transforming solar energy into chemical energy, (photo)electrochemical water splitting has attracted a great deal of interest for decades.[1] Water splitting is a combination of two half-reactions, the oxygen evolution reaction (OER) at the (photo)anode and the hydrogen evolution reaction (HER) at the cathode of a (photo)-electrochemical cell. Of these two half-reactions, the OER is the major obstacle because of its sluggish kinetics. Furthermore, state-of-the-art OER catalysts usually contain precious metals, e.g., Ir and Ru, which are not convenient for large-scale applications. Active OER catalysts using only Earth's abundant elements, e.g., Fe, Ni, or another 3d transition metal, are highly desirable.

Nickel oxide (NiO_x) electrodes have been widely used in alkaline batteries.[2−6] It has long been known that iron impurities in nickel oxide electrodes facilitate the OER,[7−10] which is a side reaction during the battery charging process. Inspired by this finding, since the 1980s some researchers have redirected their work originally focused on nickel oxide battery applications toward iron–nickel composite oxide catalysts for the OER under aqueous alkaline conditions.[9−11] Many experiments have shown that mixed iron–nickel oxides are promising anode materials for the OER.[12−18] Various groups[9,10] showed that the overpotential decreases by ∼150 mV after ∼10% Fe is doped into NiO_x. Recently, Trotochaud et al.[14,19] reported that the OER activity of $Fe_{0.1}Ni_{0.9}O_x$ is comparable to that of $Ba_{0.5}Sr_{0.5}Co_{0.8}Fe_{0.2}O_{3-\delta}$, the best-known OER catalyst in basic media.[20] Similarly, Gong et al. reported that mixed Ni–Fe oxide on oxidized multiwalled carbon nanotubes has a higher OER activity than commercial Ir/C catalysts.[12]

Despite extensive studies, the origin of the high OER activity of Fe-doped nickel oxides is not fully understood. This is largely due to the uncertainty in the composition and structure of the active NiO_x phase under OER conditions. During charging and discharging, a variety of phase transformations can occur between different nickel hydroxide variants. As shown by the Bode's diagram[21] in Scheme 1, β-NiOOH is formed during charging, followed by γ-NiOOH under overcharging conditions.[21] While it is generally believed that β-NiOOH is the active OER phase,[22,23] recently Bediako et al. argued that γ-NiOOH might be more efficient.[24] By spectroscopic measurements, Landon et al.[15] found that Fe-doped NiO_x (briefly denoted Fe-NiO_x) contains the spinel $NiFe_2O_4$ phase and proposed that this is responsible for the robust OER activity of

Scheme 1. Bode's Diagram for $Ni(OH)_2$–NiOOH Redox Transformations

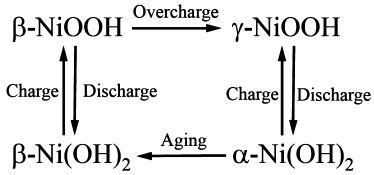

Received: December 27, 2013
Revised: February 27, 2014
Published: March 3, 2014

Fe-NiO_x. Using $[Ru(bpy)_3]^{2+}$ and $S_2O_8^{2-}$ as a photosensitizer and reducing agent, respectively, Hong et al.[25] showed that the OER activity of $NiFe_2O_4$ is similar to that of Co_3O_4, another promising OER catalyst.[26]

At variance with the numerous experimental investigations, theoretical studies on NiO_x are still scarce.[27] To identify the active phase during the OER on NiO_x and Fe-NiO_x, we have investigated the mechanisms of the OER on several nickel and iron−nickel (hydro)oxide surfaces, namely, pure and Fe-doped β-NiOOH$(01\bar{1}5)$ and γ-NiOOH(101), as well as $NiFe_2O_4(001)$ and, for comparison, $Fe_3O_4(001)$. The rationale for choosing these specific surfaces will be given in section 2, where the investigated models are described. Among the investigated surfaces, Fe-doped β-NiOOH$(01\bar{1}5)$ has the lowest overpotential, followed by $NiFe_2O_4(001)$, consistent with the observed increase in the OER activity of NiO_x when it is doped with Fe.

2. METHODS, MODELS, AND CALCULATION DETAILS

Spin-polarized density functional theory (DFT) calculations were performed in the plane wave and ultrasoft pseudopotential[28] framework as implemented in QUANTUM-ESPRESSO.[29] The PBE[30] functional with on-site Coulomb repulsion was utilized, and the effective U-J terms, from linear response theory,[31] were 3.3 and 5.5 eV for Fe and Ni, respectively. The kinetic energy cutoffs of 30 and 300 Ry were chosen for the wave functions and augmented charge densities, respectively. The Broyden−Fletcher−Goldfarb−Shanno (BFGS) method was employed for geometry relaxations until the maximal forces on each relaxed atom were <0.001 Ry/bohr.

Both $NiFe_2O_4$ and Fe_3O_4 have an inverse spinel structure and are ferrimagnetic.[32,33] The computed electronic densities of states are reported in Figure S1 of the Supporting Information. These show that Fe_3O_4 is half-metallic while $NiFe_2O_4$ is a semiconductor, consistent with previous computational studies.[32,33] Calculations of the OER energetics were performed for the (001) surface, which is the most frequently exposed surface of the spinel structure (see Figure 1a). Symmetric, non-stoichiometric slabs were utilized, with eight type B and seven type A layers[34] and surface unit cells with dimensions of 6.002 Å × 6.002 Å and 5.906 Å × 5.906 Å for Fe_3O_4 and $NiFe_2O_4$, respectively, corresponding to a total of 55 atoms per unit cell. There are two 5-fold coordinated Fe cations (Fe_{5c}) and four 3-fold coordinated oxygen anions (O_{3c}) per unit cell on the $Fe_3O_4(001)$ surface, while $NiFe_2O_4(001)$ exposes one Fe_{5c}, one Ni_{5c}, and four O_{3c} ions per unit cell. For these surface slabs, a 3 × 3 × 1 Monkhorst−Pack k-point mesh was utilized for energy and structural calculations.

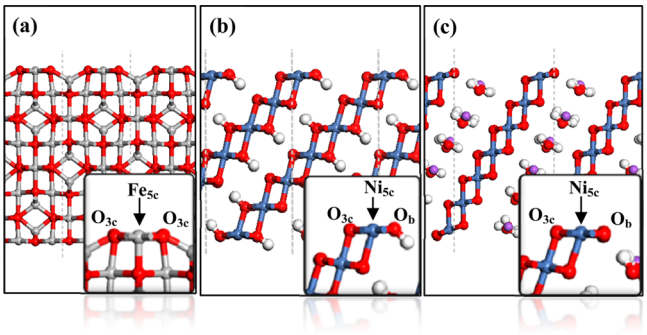

Figure 1. Slab models for (a) $Fe_3O_4(001)$, (b) β-NiOOH$(01\bar{1}5)$, and (c) γ-NiOOH(101). O, H, Fe, and Ni atoms are colored red, white, gray, and blue, respectively. Na ions in panel c are colored purple. Insets show the various types of surface atoms, Fe_{5c}, Ni_{5c}, O_{3c}, and O_b. Vertical dashed lines indicate the surface unit cells.

For β- and γ-NiOOH, the precise structures are not well-known, because of the poor quality of the available X-ray diffraction patterns. However, it is generally agreed that for β-NiOOH no major modification of the hexagonal β-$Ni(OH)_2$ structure takes place upon oxidation,[35] while γ-NiOOH is known to contain water molecules and alkali metal ions originating from the alkaline electrolyte.[35] From the results of a series of charging and discharging experiments on various forms of $Ni(OH)_2$, Barnard et al.[3] concluded that γ-NiOOH has a Ni oxidation state of 3.3−3.67 while β-NiOOH has a Ni oxidation state of 2.7−3.0. In this work, we constructed the unit cells of β-NiOOH and γ-NiOOH ($Na_{0.33}NiO_2{\cdot}0.67H_2O$) based on previous experimental data and theoretical calculations;[36−38] atomic coordinates are given in the Supporting Information. In our optimized unit cell, the intersheet distance of γ-NiOOH is 7.0 Å, which is well consistent with the experimental value of ∼7 Å.[38,39] The oxidation state of Ni is +3 for β-NiOOH and +3.66 for γ-NiOOH. The calculated electronic densities of states (Figure S1 of the Supporting Information) show that both β-NiOOH and γ-NiOOH are half-metallic, which is attributed to the partially occupied e_g orbitals.

Recent theoretical studies of CoO_x, which has the same layered structure as NiO_x, have found that the natural (0001) surface has a high overpotential and is thus inactive for the OER[40] while the higher-Miller index $(01\bar{1}2)$ and $(01\bar{1}4)$ surfaces are active.[41,42] This can be understood by considering that on the (0001) surface the exposed Co atoms are 6-fold coordinated, so they can form only very weak bonds with the various OER intermediates.[40] On higher-index surfaces, as well as at step edges, instead, the Co atoms are not fully coordinated and, therefore, much more reactive. A similar argument can be also applied to β-NiOOH and γ-NiOOH. We thus study their reactivity by considering two higher-index surfaces, notably β-NiOOH$(01\bar{1}5)$ and γ-NiOOH(101), that we model using monoclinic surface cells with dimensions of 5.978 Å × 6.353 Å (γ = 76.4°) and 8.457 Å × 8.650 Å (γ = 80.2°), respectively. The slab thickness was ∼13 Å. The β-NiOOH$(01\bar{1}5)$ surface exposes two Ni_{5c}, two O_{3c}, and two O_b ions, per surface unit cell, while there are three exposed Ni_{5c}, three O_{3c}, and three O_b ions per surface unit cell on γ-NiOOH(101) (see Figure 1). One exposed Ni_{5c} was replaced by Fe_{5c} to model Fe-doped NiO_x. The total number of atoms per unit cell was 56 and 105 for β-NiOOH$(01\bar{1}5)$ and γ-NiOOH(101), respectively. For these surface slabs, 3 × 3 × 1 and 2 × 2 × 1 Monkhorst−Pack k-point meshes were utilized for energy and structural calculations. The different k-point meshes were chosen to produce results with similar precision for the different surfaces.

The OER free energy profiles were derived using the same scheme utilized in previous studies.[43−46] We used the standard hydrogen electrode (SHE) as a reference, so the proton ($G[H^+]$) and electron free energies ($G[e^-]$) are replaced by $G[H_2]$-|e| U, where $G[H_2]$ is the free energy of H_2 and U is the electrode potential versus the SHE (pH 0, p = 1 bar, T = 298.15 K). For O_2, the free energy is expressed as $G[O_2] = 4.92$ eV + $2G[H_2O] - 2G[H_2]$, according to the OER equilibrium under standard conditions. Because the theoretical overpotential does not depend on pH, all the free energy results are calculated at pH 0 unless explicitly mentioned otherwise. As an approximate description of solvation effects, each exposed metal ion was

dx.doi.org/10.1021/cs401245q | ACS Catal. 2014, 4, 1148−1153

covered by at least one surface-adsorbed species, e.g., OH, O, H_2O, etc. Although very simplified, this model is generally considered to be adequate for capturing trends in structurally related systems.[40,47]

3. RESULTS AND DISCUSSION

3.1. Surface Structure in the Presence of an Adsorbed Water Monolayer. The stable structures of an adsorbed water monolayer (ML) on $Fe_3O_4(001)$, $NiFe_2O_4(001)$, pure and Fe-doped β-NiOOH(01$\bar{1}$5), and pure and Fe-doped γ-NiOOH(101) are reported in Table S1 of the Supporting Information. For both $Fe_3O_4(001)$ and $NiFe_2O_4(001)$, the most stable structures are mixed molecular-dissociated monolayers, specifically, $Fe_3O_4(001)$ ($^1/_2$ML HO_{3c} + $^1/_2$ML HO_t + $^1/_2$ML H_2O)[34,48,49] and $NiFe_2O_4(001)$ [$^1/_2$ ML HO_{3c} + $^1/_2$ ML HO_t(Fe) + $^1/_2$ ML H_2O], where HO_t/HO_t(Fe) is a terminal hydroxyl on top of a Ni/Fe ion and HO_{3c} is a three-coordinated hydroxyl. For pure and Fe-doped β-NiOOH(01$\bar{1}$5), the adsorbed monolayers are fully molecular (1 ML H_2O). On γ-NiOOH(101), it is energetically favorable to replace the sodium ion at the edge with a proton to form a bridging hydroxyl (HO_b), while one of two water molecules is dissociated into an O_{ad} and two HO_b (see state **11** in Figure 2 and the Supporting Information for details). As a result, a phase with 1 ML H_2O + 1 ML HO_b + 0.33 ML O_{ad} is formed, which is 1.11 eV more stable than the as-cleaved surface (at pH 14). After two consecutive proton transfer processes, however, this structure changes into 1 ML H_2O + 1 ML HO_b (see state **9** in Figure 2). The latter is chosen as the initial state of the OER on pure and Fe-doped γ-NiOOH(001).

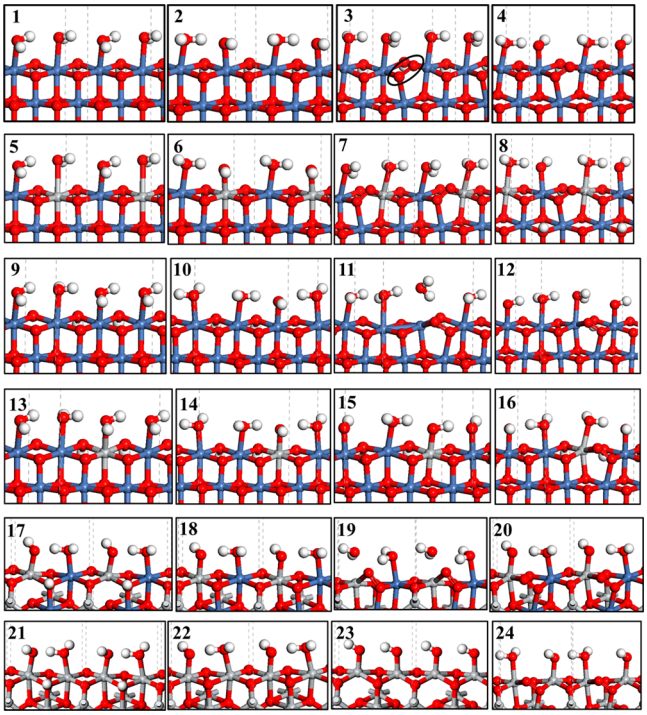

Figure 2. Optimized structures of the OER intermediates: **1**–**4**, β-NiOOH(01$\bar{1}$5); **5**–**8**, Fe doped β-NiOOH(01$\bar{1}$5); **9**–**12**, γ-NiOOH-(101); **13**–**16**, Fe-doped γ-NiOOH(101); **17**–**20**, $NiFe_2O_4(001)$; **21**–**24**, $Fe_3O_4(001)$. Oxygen, hydrogen, iron, and nickel atoms are colored red, white, gray, and blue, respectively. Vertical dashed lines indicate the surface unit cells. The black ellipse in **3** highlights the O–O bond between the O adatom and a surface lattice O_{3c}.

3.2. OER Mechanisms. To map out the OER reaction pathway, we took a recursive trial-and-error approach, in which we investigated each "likely" oxidation channel by adding H_2O to the surface and then removing H (proton/electron pair) stepwise until an O_2 species was produced. In the following, we describe the calculated lowest-energy pathways for OER on the various surfaces, as shown in Figure 2 and Table 1.

For β-NiOOH(01$\bar{1}$5), the rate-determining step (RDS) is the first release of a proton from an adsorbed water molecule, leaving an adsorbed OH (state **2**); the corresponding overpotential (η) is 0.46 V. After the second release of a proton from the adsorbed OH, an O–O bond forms between the O adatom and a surface lattice O_{3c}, while a solvent water molecule adsorbs at the exposed Ni_{5c} adjacent to the O–O species (state **3**). Another adsorbed H_2O loses a proton and transforms into an adsorbed OH (state **4**). After the fourth proton release, O_2 forms and desorbs from the surface, thus allowing another solvent water molecule to adsorb on the exposed Ni_{5c}. In this way, the 1 ML H_2O covered surface is recovered (state **1**). Reaction pathways very similar to that on β-NiOOH(01$\bar{1}$5) are found also for Fe-doped β-NiOOH(01$\bar{1}$5), where the RDS is the second proton release with an η of 0.26 V, and pure γ-NiOOH(101), where the RDS is the third proton release with an η of 0.52 V.

A slightly different OER mechanism is found for Fe-doped γ-NiOOH(101). After the first proton release (state **14**), the water molecule adjacent to the adsorbed OH also loses a proton and transforms into another adsorbed OH (state **15**). This is the RDS, with an η of 0.48 V. After release of the third proton from an adsorbed OH, an O–O bond forms between the O adatom and a surface lattice O_{3c}, while a solvent H_2O adsorbs at the exposed Ni_{5c} adjacent to the O–O species (state **16**). After release of the fourth proton, O_2 desorbs from the surface, followed by the adsorption of another H_2O on the exposed Ni_{5c} to recover the 1 ML H_2O covered surface (state **13**). A similar pathway is found also for $Fe_3O_4(001)$, for which the overpotential is quite large (η = 0.70 V).

Finally, the first proton release is the RDS on $NiFe_2O_4(001)$ (state **18**), and the overpotential (η) is 0.42 V. After the second release of a proton from the adsorbed OH, an O–O bond is formed between the O adatom and a surface lattice oxygen, while a solvent water molecule adsorbs at the exposed Fe_{5c} adjacent to the O–O species (state **19**). Subsequently, the newly adsorbed water molecule releases the third proton, transforming into an adsorbed OH (state **20**). After release of the fourth proton, O_2 desorbs from the surface, followed by water adsorption on the exposed Fe_{5c} to re-form state **17**. The calculated overpotential (η = 0.42 V) is consistent with the experimental onset overpotential of 0.43 V.[25]

3.3. Active Phase for Enhanced OER Activity on Fe-Doped NiO_x. From Table 1, we can see that the computed overpotentials increase in the following order: Fe-doped β-NiOOH(01$\bar{1}$5) (0.26 V) < $NiFe_2O_4(001)$ (0.42 V) < β-NiOOH(01$\bar{1}$5) (0.46 V) < Fe-doped γ-NiOOH(001) (0.48 V) < γ-NiOOH(101) (0.52 V) < $Fe_3O_4(001)$ (0.70 V). In the case of pure NiO_x, the difference between the computed overpotentials of β-NiOOH(01$\bar{1}$5) and γ-NiOOH(101) is quite small (0.06 V). Such a small difference might explain why both β-NiOOH and γ-NiOOH have been proposed as the active phase of pure NiO_x by different authors.[22−24] Although our study is restricted to only one surface of each material, the

dx.doi.org/10.1021/cs401245q | ACS Catal. 2014, 4, 1148−1153

Table 1. Energetics of the OER on Ni, Ni−Fe, and Fe (Hydro)oxide Surfaces

elementary step	ΔE (eV)	$\Delta H(0\rightarrow298K)$ (eV)	ΔZPE (eV)	$-T\Delta S$ (eV)	ΔG (eV)
		β-NiOOH(01$\bar{1}$5)			
1 + $h^+ \rightarrow$ **2** + H^+	2.06	0.04	−0.21	−0.20	1.69
2 + $h^+ + H_2O \rightarrow$ **3** + H^+	0.67	−0.06	0.02	0.47	1.10
3 + $h^+ \rightarrow$ **4** + H^+	1.79	0.04	−0.22	−0.20	1.41
4 + $h^+ + H_2O \rightarrow$ **1** + $H^+ + O_2$	0.93	0.04	−0.09	−0.16	0.72
		Fe-Doped β-NiOOH(01$\bar{1}$5)			
5 + $h^+ \rightarrow$ **6** + H^+	1.71	0.04	−0.21	−0.20	1.34
6 + $h^+ + H_2O \rightarrow$ **7** + H^+	1.06	−0.06	0.02	0.47	1.49
7 + $h^+ \rightarrow$ **8** + H^+	1.67	0.04	−0.22	−0.20	1.29
8 + $h^+ + H_2O \rightarrow$ **5** + $H^+ + O_2$	1.01	0.04	−0.09	−0.16	0.80
		γ-NiOOH(101)			
9 + $h^+ \rightarrow$ **10** + H^+	1.76	0.04	−0.21	−0.20	1.39
10 + $h^+ + H_2O \rightarrow$ **11** + H^+	0.94	−0.06	0.02	0.47	1.37
11 + $h^+ \rightarrow$ **12** + H^+	2.13	0.04	−0.22	−0.20	1.75
12 + $h^+ + H_2O \rightarrow$ **9** + $H^+ + O_2$	0.62	0.04	−0.09	−0.16	0.41
		Fe-Doped γ-NiOOH(101)			
13 + $h^+ \rightarrow$ **14** + H^+	1.52	0.04	−0.21	−0.20	1.15
14 + $h^+ \rightarrow$ **15** + H^+	2.09	0.04	−0.22	−0.20	1.71
15 + $h^+ + H_2O \rightarrow$ **16** + H^+	1.16	−0.06	0.02	0.47	1.59
16 + $h^+ + H_2O \rightarrow$ **13** + $H^+ + O_2$	0.68	0.04	−0.09	−0.16	0.47
		$NiFe_2O_4$(001)			
17 + $h^+ \rightarrow$ **18** + H^+	2.02	0.04	−0.21	−0.20	1.65
18 + $h^+ + H_2O \rightarrow$ **19** + H^+	1.07	−0.06	0.02	0.47	1.50
19 + $h^+ \rightarrow$ **20** + H^+	1.77	0.04	−0.22	−0.20	1.39
20 + $h^+ + H_2O \rightarrow$ **17** + $H^+ + O_2$	0.59	0.04	−0.09	−0.16	0.38
		Fe_3O_4(001)			
21 + $h^+ \rightarrow$ **22** + $H^+ + O_2$	1.21	0.04	−0.21	−0.20	0.84
22 + $h^+ \rightarrow$ **23** + H^+	2.31	0.04	−0.22	−0.20	1.93
23 + $h^+ + H_2O \rightarrow$ **24** + H^+	1.31	−0.06	0.02	0.47	1.74
24 + $h^+ + H_2O \rightarrow$ **21** + $H^+ + O_2$	0.62	0.04	−0.09	−0.16	0.41

investigated surfaces are indeed (among) the most active for β-NiOOH and γ-NiOOH. Nonetheless, more comprehensive theoretical investigations and more experimental data would be desirable to sort out which of the two NiOOH structures is the active phase of the OER.

For Fe-doped NiO_x, our results predict a remarkably low overpotential for Fe-doped β-NiOOH(01$\bar{1}$5) (η = 0.26 V). Such an overpotential is even lower than that of RuO_2 (0.36 V),[45,50] a known efficient OER catalyst. This finding is consistent with the experimental observation that the OER activity of Fe-NiO_x can be as high as that of $Ba_{0.5}Sr_{0.5}Co_{0.8}Fe_{0.2}O_{3-\delta}$,[14] the best OER catalyst in basic media.[20] Our calculations also predict that $NiFe_2O_4$ is an efficient OER catalyst, even though it is less active than Fe-doped β-NiOOH, whereas for Fe-doped γ-NiOOH, the predicted overpotential is slightly higher than that of pure β-NiOOH. Thus, Fe-doped γ-NiOOH is unlikely to be the active component of Fe-NiO_x. The predicted relative overpotentials of $NiFe_2O_4$, Fe-doped β-NiOOH, and Fe-doped γ-NiOOH can also explain the experimental observation that the OER activity for Fe-doped NiO_x decreases in the following order: 10% Fe > 5% Fe > 20% Fe > NiO_x.[15] At low concentrations, Fe doping would not change the phase of NiO_x, and thus, Fe atoms are mainly doped into the β- or γ-$Ni(OH)_2$ phase, ultimately leading to Fe-doped β-NiOOH, which has a high OER activity. When the Fe concentration increases, Fe atoms transfer from NiO_x to the less active $NiFe_2O_4$ phase, as shown by the XRD patterns in ref 15. While both Fe-doped β-NiOOH and $NiFe_2O_4$ contribute to the enhanced OER activity of Fe-NiO_x relative to that of pure NiO_x, higher Fe doping levels lead to a higher content of $NiFe_2O_4$, which has activity lower than that of Fe-doped β-NiOOH. The activity at very high Fe doping levels can thus be lower than at low and moderate Fe concentrations.

3.4. Strategies To Improve the OER Activity on NiO_x.

On the basis of the analysis presented above, it appears that the most straightforward way to improve the OER performance of iron−nickel oxides would be to increase the concentration of Fe-doped β-NiOOH. This can be achieved using moderate Fe doping levels that do not change the layered structure of NiO_x. Aging can also increase the concentration of Fe-doped β-NiOOH and thus the OER activity, assuming that low to moderate Fe doping concentrations do not change the Bode's diagram (Scheme 1). This deduction is indirectly supported by CV experiments[9] showing that while the OER activity of NiO_x decreases after 100 CV cycles, the deactivation effect is suppressed for Fe-doped NiO_x. This may result from the fact that in aged Fe-NiO_x more Fe-doped β-NiOOH is formed, canceling out the deactivation of repeated CV cycles.

It is also interesting to examine the effect of different dopants on the OER activity of NiO_x. Because the active phase for pure NiO_x is β-NiOOH, for which the first proton release is the rate-determining step, it is essential to lower the barrier of the first proton release to improve the performance of NiO_x. We can estimate the effect of different dopants on the activity of NiO_x by comparing the barriers of first proton release on the pure oxides of the various dopant elements. Considering Fe, Co, and Ni as an example, the barrier of the first proton release on the pure oxides satisfies Fe_3O_4 < β-NiOOH < CoOOH, where we

dx.doi.org/10.1021/cs401245q | ACS Catal. 2014, 4, 1148−1153

use the values in Table 1 for Fe_3O_4 and β-NiOOH, whereas for CoOOH, we use the computed barrier of the first proton release (2.01 eV) on CoOOH($01\bar{1}5$).[40] This suggests that Fe doping would enhance the OER activity of NiO_x while Co doping would make it slower, although on the basis of rather rough estimates, this prediction appears to work quite well. In real applications, Fe-doped NiO_x is indeed utilized to catalyze the OER, while Co-doped NiO_x is used in alkaline batteries to suppress the OER.

4. CONCLUSIONS

This paper presents thorough calculations of the OER energetic pathways on several surfaces of Ni and Ni−Fe oxides, which could represent the active phase of NiO_x under OER conditions. The computed overpotentials on these oxides increase in the following order: Fe-doped β-NiOOH (0.26 V) < $NiFe_2O_4$ (0.42 V) < β-NiOOH (0.46 V) < Fe-doped γ-NiOOH (0.48 V) < γ-NiOOH (0.52 V) < Fe_3O_4 (0.70 V). The most important result of this work is the identification of Fe-doped β-NiOOH as a robust catalyst for electrocatalytic water oxidation. On the basis of the computed overpotential, Fe-doped β-NiOOH is predicted to be even more active than RuO_2, a well-established catalyst for the OER. $NiFe_2O_4$ is another efficient OER catalyst, but less active than Fe-doped β-NiOOH, according to our study. Both Fe-doped β-NiOOH and $NiFe_2O_4$ could contribute to the OER catalyst's active phase of Fe-doped NiO_x. Assuming that Bode's diagram is valid for Fe-doped NiO_x, our results suggest that the OER activity of NiO_x can be enhanced through low to moderate Fe doping levels and aging.

■ ASSOCIATED CONTENT

Supporting Information

Electronic structures of bulk Fe_3O_4, $NiFe_2O_4$, β-NiOOH, and γ-NiOOH; bulk structural parameters and atomic coordinates of β-NiOOH and γ-NiOOH; and surface structure of γ-NiOOH in the presence of an adsorbed water monolayer. This material is available free of charge via the Internet at http://pubs.acs.org.

■ AUTHOR INFORMATION

Corresponding Authors

*E-mail: yefeil@princeton.edu.
*E-mail: aselloni@princeton.edu.

Notes

The authors declare no competing financial interest.

■ ACKNOWLEDGMENTS

This work was supported by DoE-BES, Division of Chemical Sciences, Geosciences and Biosciences, via Grant DE-FG02-12ER16286. We used resources of the National Energy Research Scientific Computing Center (DoE Contract DE-AC02-05CH11231). We also acknowledge use of the the TIGRESS high-performance computer center at Princeton University.

■ REFERENCES

(1) Fujishima, A.; Honda, K. *Nature* **1972**, *238*, 37−38.
(2) Briggs, G. W. D.; Jones, E.; Wynne-Jones, W. F. K. *Trans. Faraday Soc.* **1955**, *51*, 1433−1442.
(3) Barnard, R.; Randell, C. F.; Tye, F. L. *J. Appl. Electrochem.* **1980**, *10*, 109−125.
(4) Micka, K.; Mrha, J.; VondrTye, F. *J. Power Sources* **1982**, *8*, 351−357.
(5) Oshitani, M.; Sasaki, Y.; Takashima, K. *J. Power Sources* **1984**, *12*, 219−231.
(6) Carpenter, M. K.; Corrigan, D. A. *J. Electrochem. Soc.* **1989**, *136*, 1022−1026.
(7) Casey, E. J.; Dubois, A. R.; Lake, P. E.; Moroz, W. J. *J. Electrochem. Soc.* **1965**, *112*, 371−383.
(8) Corrigan, D. A.; Bendert, R. M. *J. Electrochem. Soc.* **1989**, *136*, 723−728.
(9) Corrigan, D. A. *J. Electrochem. Soc.* **1987**, *134*, 377−384.
(10) Miller, E. L.; Rocheleau, R. E. *J. Electrochem. Soc.* **1997**, *144*, 3072−3077.
(11) Młynarek, G.; Paszkiewicz, M.; Radniecka, A. *J. Appl. Electrochem.* **1984**, *14*, 145−149.
(12) Gong, M.; Li, Y.; Wang, H.; Liang, Y.; Wu, J. Z.; Zhou, J.; Wang, J.; Regier, T.; Wei, F.; Dai, H. *J. Am. Chem. Soc.* **2013**, *135*, 8452−8455.
(13) Smith, R. D. L.; Prévot, M. S.; Fagan, R. D.; Zhang, Z.; Sedach, P. A.; Siu, M. K. J.; Trudel, S.; Berlinguette, C. P. *Science* **2013**, *340*, 60−63.
(14) Trotochaud, L.; Ranney, J. K.; Williams, K. N.; Boettcher, S. W. *J. Am. Chem. Soc.* **2012**, *134*, 17253−17261.
(15) Landon, J.; Demeter, E.; İnoğlu, N.; Keturakis, C.; Wachs, I. E.; Vasić, R.; Frenkel, A. I.; Kitchin, J. R. *ACS Catal.* **2012**, *2*, 1793−1801.
(16) Smith, R. D. L.; Prévot, M. S.; Fagan, R. D.; Trudel, S.; Berlinguette, C. P. *J. Am. Chem. Soc.* **2013**, *135*, 11580−11586.
(17) Li, X.; Walsh, F. C.; Pletcher, D. *Phys. Chem. Chem. Phys.* **2011**, *13*, 1162−1167.
(18) Louie, M. W.; Bell, A. T. *J. Am. Chem. Soc.* **2013**, *135*, 12329−12337.
(19) Trotochaud, L.; Mills, T. J.; Boettcher, S. W. *J. Phys. Chem. Lett.* **2013**, *4*, 931−935.
(20) Suntivich, J.; May, K. J.; Gasteiger, H. A.; Goodenough, J. B.; Shao-Horn, Y. *Science* **2011**, *334*, 1383−1385.
(21) Bode, H.; Dehmelt, K.; Witte, J. *Electrochim. Acta* **1966**, *11*, 1079−1087.
(22) Lyons, M. E. G.; Brandon, M. P. *Int. J. Electrochem. Sci.* **2008**, *3*, 1386−1424.
(23) Lu, P. W. T.; Srinivasan, S. *J. Electrochem. Soc.* **1978**, *125*, 1416−1422.
(24) Bediako, D. K.; Lassalle-Kaiser, B.; Surendranath, Y.; Yano, J.; Yachandra, V. K.; Nocera, D. G. *J. Am. Chem. Soc.* **2012**, *134*, 6801−6809.
(25) Hong, D.; Yamada, Y.; Nagatomi, T.; Takai, Y.; Fukuzumi, S. *J. Am. Chem. Soc.* **2012**, *134*, 19572−19575.
(26) Kanan, M. W.; Nocera, D. G. *Science* **2008**, *321*, 1072−1075.
(27) Hermet, P.; Gourrier, L.; Bantignies, J. L.; Ravot, D.; Michel, T.; Deabate, S.; Boulet, P.; Henn, F. *Phys. Rev. B* **2011**, *84*, 235211.
(28) Vanderbilt, D. *Phys. Rev. B* **1990**, *41*, 7892−7895.
(29) Giannozzi, P.; Baroni, S.; Bonini, N.; Calandra, M.; Car, R.; Cavazzoni, C.; Ceresoli, D.; Chiarotti, G. L.; Cococcioni, M.; Dabo, I.; Dal Corso, A.; de Gironcoli, S.; Fabris, S.; Fratesi, G.; Gebauer, R.; Gerstmann, U.; Gougoussis, C.; Kokalj, A.; Lazzeri, M.; Martin-Samos, L.; Marzari, N.; Mauri, F.; Mazzarello, R.; Paolini, S.; Pasquarello, A.; Paulatto, L.; Sbraccia, C.; Scandolo, S.; Sclauzero, G.; Seitsonen, A. P.; Smogunov, A.; Umari, P.; Wentzcovitch, R. M. *J. Phys.: Condens. Matter* **2009**, *21*, 395502.
(30) Perdew, J. P.; Burke, K.; Ernzerhof, M. *Phys. Rev. Lett.* **1996**, *77*, 3865−3868.
(31) Cococcioni, M.; de Gironcoli, S. *Phys. Rev. B* **2005**, *71*, 035105.
(32) Szotek, Z.; Temmerman, W. M.; Ködderitzsch, D.; Svane, A.; Petit, L.; Winter, H. *Phys. Rev. B* **2006**, *74*, 174431.
(33) Fritsch, D.; Claude, E. *J. Phys.: Conf. Ser.* **2011**, *292*, 012014.
(34) Kendelewicz, T.; Kaya, S.; Newberg, J. T.; Bluhm, H.; Mulakaluri, N.; Moritz, W.; Scheffler, M.; Nilsson, A.; Pentcheva, R.; Brown, G. E. *J. Phys. Chem. C* **2013**, *117*, 2719−2733.
(35) Oliva, P.; Leonardi, J.; Laurent, J. F.; Delmas, C.; Braconnier, J. J.; Figlarz, M.; Fievet, F.; Guibert, A. d. *J. Power Sources* **1982**, *8*, 229−255.

(36) Casas-Cabanas, M.; Canales-Vázquez, J.; Rodríguez-Carvajal, J.; Palacín, M. R. *J. Am. Chem. Soc.* **2007**, *129*, 5840−5842.
(37) Van der Ven, A.; Morgan, D.; Meng, Y. S.; Ceder, G. *J. Electrochem. Soc.* **2006**, *153*, A210−A215.
(38) Yang, X.; Takada, K.; Itose, M.; Ebina, Y.; Ma, R.; Fukuda, K.; Sasaki, T. *Chem. Mater.* **2008**, *20*, 479−485.
(39) Bardé, F.; Palacín, M. R.; Beaudoin, B.; Tarascon, J. M. *Chem. Mater.* **2005**, *17*, 470−476.
(40) Chen, J.; Selloni, A. *J. Phys. Chem. C* **2013**, *117*, 20002−20006.
(41) García-Mota, M.; Bajdich, M.; Viswanathan, V.; Vojvodic, A.; Bell, A. T.; Nørskov, J. K. *J. Phys. Chem. C* **2012**, *116*, 21077−21082.
(42) Bajdich, M.; García-Mota, M.; Vojvodic, A.; Nørskov, J. K.; Bell, A. T. *J. Am. Chem. Soc.* **2013**, *135*, 13521−13530.
(43) Li, Y.-F.; Liu, Z.-P.; Liu, L.; Gao, W. *J. Am. Chem. Soc.* **2010**, *132*, 13008−13015.
(44) Valdeés, A.; Qu, Z. W.; Kroes, G. J.; Rossmeisl, J.; Nørskov, J. K. *J. Phys. Chem. C* **2008**, *112*, 9872−9879.
(45) Rossmeisl, J.; Qu, Z. W.; Zhu, H.; Kroes, G. J.; Nørskov, J. K. *J. Electroanal. Chem.* **2007**, *607*, 83−89.
(46) Li, Y.-F.; Liu, Z.-P. *J. Am. Chem. Soc.* **2011**, *133*, 15743−15752.
(47) Man, I. C.; Su, H.-Y.; Calle-Vallejo, F.; Hansen, H. A.; Martínez, J. I.; Inoglu, N. G.; Kitchin, J.; Jaramillo, T. F.; Nørskov, J. K.; Rossmeisl, J. *ChemCatChem* **2011**, *3*, 1159−1165.
(48) Mulakaluri, N.; Pentcheva, R.; Scheffler, M. *J. Phys. Chem. C* **2010**, *114*, 11148−11156.
(49) Mulakaluri, N.; Pentcheva, R.; Wieland, M.; Moritz, W.; Scheffler, M. *Phys. Rev. Lett.* **2009**, *103*, 176102.
(50) Fang, Y.-H.; Liu, Z.-P. *J. Am. Chem. Soc.* **2010**, *132*, 18214−18222.